Mixed-basis cluster expansion for thermodynamics of bcc alloys

Volker Blum and Alex Zunger

National Renewable Energy Laboratory, 1617 Cole Boulevard, Golden, Colorado 80401, USA

(Received 30 December 2003; revised manuscript received 12 April 2004; published 25 October 2004)

To predict the ground-state structures and finite-temperature properties of an alloy, the total energies of many different atomic configurations $\boldsymbol{\sigma} \equiv \{S_i; i=1,\ldots,N\}$, with N sites i occupied by atom A ($S_i=-1$), or B ($S_i=+1$), must be calculated accurately and rapidly. Direct local-density approximation (LDA) calculations provide the required accuracy, but are not practical because they are limited to small cells and only a few of the 2^N possible configurations. The "mixed-basis cluster expansion" (MBCE) method allows to parametrize LDA configurational energetics $E_{\mathrm{LDA}}(S_i)$ 2

formalism for many fcc-based alloys. In this paper, we describe how to construct a deterministic, LDA-quality MBCE, i.e., how (i) and (ii) are addressed by a systematic assessment of the predictive power of a given CE within a set of input ΔH_{LDA} (cross validation[21,22]), and the iterative enlargement of the LDA input data base as a whole.[10,22] We extend the formalism to a *bcc-based* binary alloy, Mo-Ta. In addition to predicted ground states,[23] we address the system's finite-T thermodynamics (order-disorder transitions, short-range order, and random alloy limit) in relation to experimental work.[24,25]

B. Why Mo-Ta

The most prominent group of fully bcc-based binary alloys (no known phases based on a different type of underlying lattice, e.g., fcc) is formed from the refractory elements Nb, Ta, Mo, and W, located in groups VA and VIA of the periodic system of elements. Figure 1 summarizes some of their pertinent properties.[25–30] The atomic size mismatch of all six possible binary alloys formed between them is below 5%. Their experimental phase diagrams show only continuous bcc (A2) solid solutions,[31] so it is not known if at lower T these form any long-range ordered compounds, or phase separate. Regarding *short*-range order in the solid solution, the only available experimental report pertains to Mo-Ta,[24] where x-ray diffuse scattering showed clear (100)-centric intensity for 21% and 37% Ta. For Mo-Nb,[26] Mo-Ta,[25] and Ta-W,[27] negative enthalpies of mixing were observed, with Mo-Ta giving the most negative value $\Delta H_{\mathrm{exp}}\,\mathrm{AB} = -114$ meV . No experimental results are available for the remaining combinations, but a number of earlier semiempirical tight-binding-based calculations exist.[28–30] These sources agree upon a clearly less negative ΔH for Nb-W, and even slightly positive values for the in-group combinations Nb-Ta and Mo-W.

Where available, Fig. 1 also contains theoretical predictions regarding long-range order. Focusing on the two shortest pair interactions, the theoretical model of Sigli and Sanchez[30] predicted stable B2 order for Mo-Nb, Mo-Ta, and Ta-W. A more recent theoretical assessment of Ta-W,[32] also using two pair interactions for thermodynamics, corroborates this finding and suggests an additional $D0_3$-type ground state TaW_3 at very low T. The comparison of predicted A2-B2 transition temperatures finds Mo-Ta in the lead again, with a supposed T_c just above 1000 K.

We select Mo-Ta for this study since it shows the largest

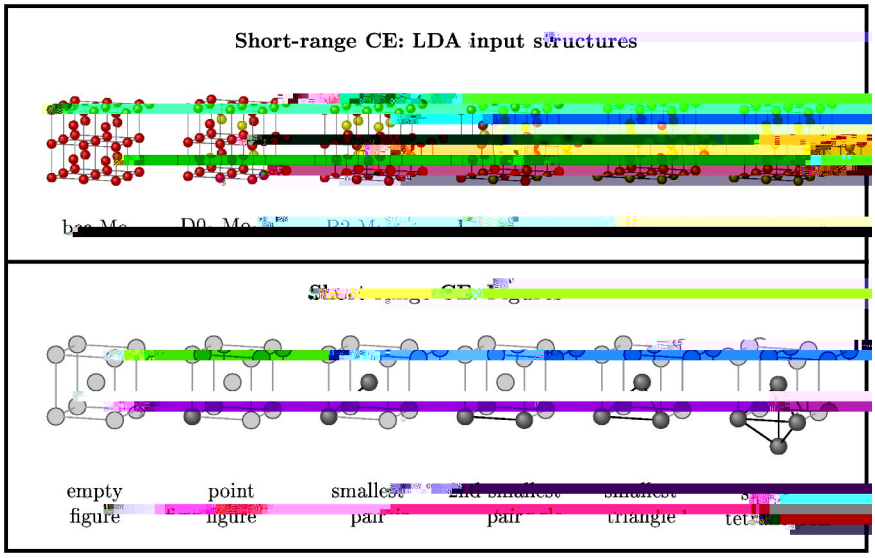

FIG. 2. (Color online) Input structures and figures for the short-range real-space CE of Mo-Ta.

The pitfall of using a small number of intuitively selected structures and figures is the resulting lack of predictive power. This can be assessed by comparing its results with a fully converged cluster expansion of Mo-Ta, described in Sec. VI, which is based on 56 input structures. The important failures of the short-range CE are: (1) Its prediction errors $\mathrm{D}H_{\mathrm{LDA}}-\mathrm{D}H_{\mathrm{CE}}$ are much larger than typical intrinsic LDA errors. For instance, the short-range CE is off by 31 meV (17% of $\mathrm{D}H_{\mathrm{LDA}}$), 31 meV (20%), and 44 meV (30%) for the three structures $\mathrm{C11_b\ Mo_2Ta}$, $\mathrm{C11_b\ MoTa_2}$, and B11 MoTa, respectively. (2) The ground-state line of the short-range CE is quantitatively far from the converged CE [see Fig. 3(b)], by up to 24 meV. Furthermore, the short-range CE misses all but the B2 ground state (missed six). (3) As pointed out by Laks *et al.*,[20] the limiting $\mathrm{D}H_{\mathrm{CE}}$ of both elements phase separated on the same coherent lattice is wrong. In a short-range CE, the predicted $\mathrm{D}H_{\mathrm{CE}}$ of $\mathrm{A}_m\mathrm{B}_n$ superlattices must converge to zero with growing period. However, simple elasticity theory shows that $\mathrm{D}H_f$, in fact, remains finite even for the fully phase-separated configuration, since both constituent element crystals must fit the same coherent underlying lattice. Even worse, the limiting $\mathrm{D}H_f$ may depend on superlattice orientation $\hat{k}$— this is known as the "$k\to 0$ singularity."

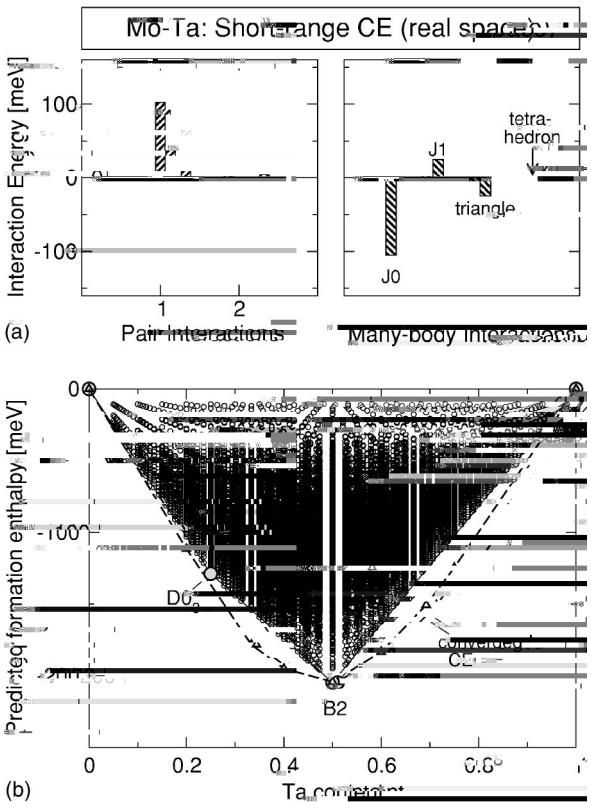

FIG. 3. (Limited(iv

In principle, there are several reasons for the qualitative failures (1)–(3): (i) *No information on coherency strain in the infinite superlattice limit is included*. The short-range CE is strictly finite ranged and therefore cannot capture the $k\to 0$ singularity. (ii) *Unphysically few figures*. Since the number of figures is limited by the number of input structures, the "cutoff" of relevant figures is mandated by fit technicalities rather than their physical decay with distance. (iii) *Limited information on atomic relaxation*. The short-range CE is based on high-symmetry ordered structures, which are prohibited by symmetry to relax, both with respect to unit-cell shape and internal coordinates. (iv) *No measure of predictive power*. The short-range CE lacks a quantitative criterion to assess the predictive power of its fitted interactions. (v) *No mechanism to extract relevant input structures and figures*. The short-range CE does not ensure either the suitability of its figure set to describe the material in question, or of its input structures to sample the configuration space optimally for a given material. As a consequence of (i)–(v), a short-range CE approach may yield deceptively "converged" results with respect to ground states and interactions, but as we see, any coincidence with truly converged results is acciden-

tal. While an intuition-based approach which already includes other "usual suspect" structures such as $C11_b$ would potentially come closer to the truth, (i)–(v) will nevertheless remain as qualitative issues. We will next discuss the conceived cure to problems (i)–(v).

III. THE MIXED-BASIS CLUSTER EXPANSION METHOD: PREVIOUS IDEAS TO OVERCOME DIFFICULTIES (I)–(V)

A. Correcting for coherency strain in the superlattice limit

We correct the "$k \rightarrow 0$" singularity of the long-period superlattice limit as described in Refs. 10, 20, and 41. We set E_{ref} of Eq. (3)

$$\delta E^{\mathrm{rel}}_{\mathrm{ord}}(\boldsymbol{\sigma}') = \sum_{s} Q_{s',s}\left(\Delta H^{\mathrm{rel}}_{\mathrm{CE}}(\boldsymbol{\sigma}) - \Delta H^{\mathrm{unrel}}_{\mathrm{CE}}(\boldsymbol{\sigma})\right). \quad (12)$$

So, the relaxation energy of the random alloy is a weighted superposition of relaxation energies of ordered compounds

$$\delta E^{\mathrm{rel}}_{\mathrm{rand}}(x) = \sum_{s} Q_{\mathrm{rand}}(\boldsymbol{\sigma})\left(\Delta H^{\mathrm{rel}}_{\mathrm{CE}}(\boldsymbol{\sigma}) - \Delta H^{\mathrm{unrel}}_{\mathrm{CE}}(\boldsymbol{\sigma})\right). \quad (13)$$

Constituent strain is implicit in this equation as a piece due to long-range relaxation, and would appear as an additional term in the actual MBCE formalism.

Recently, Ruban *et al.*[44] proposed a simplified theory of relaxation for the random alloy alone, based on breaking down each configuration into the smallest possible tetrahedra that allow for a space-filling tiling of the alloy ("effective tetrahedron model," ETM). Their approximation for $\delta E^{\mathrm{rel}}_{\mathrm{rand}}$ consists of three steps: First, $\delta E^{\mathrm{rel}}_{\mathrm{rand}}$ is written as a sum only of volume energy changes of all inequivalent tetrahedra in a given structure. Second, the volume deformation energy for a particular tetrahedron $A_{4-n}B_n$ $(n=0,\ldots,4)$ is approximated by the volume deformation energy of a crystal structure that consists exclusively of this tetrahedron type. Third, the relaxed volume of each tetrahedron type $A_{4-n}B_n$ in the random alloy at composition x is estimated from a harmonic spring model. For fcc, we have five tetrahedra corresponding to fcc A_4, $L1_2$ A_3B, $L1_0$ A_2B_2, $L1_2$ AB_3, and fcc B_4, respectively. On the bcc lattice, there are two inequivalent forms for A_2B_2, i.e., $n=1,\ldots,6$ inequivalent tetrahedron decorations $A_{4-n}B_n$, which correspond to the six structures pure bcc (A and B), $D0_3$ (A_3B and AB_3), B2 A_2B_2, and B32 A_2B_2. The complete ETM expression thus resembles Eq. (13), but with the sum limited to the six specific high-symmetry configurations, and $Q_{\mathrm{rand}}(\boldsymbol{\sigma})$ replaced by the Bernoulli probability $p^n(x)$ to find a given tetrahedron decoration n at composition x

$$\delta E^{\mathrm{rel,ETM}}_{\mathrm{rand}}(x) = \sum_{n=1}^{6} p^n(x)\left\{E^n\left(V^n_{\mathrm{rel}}(x)\right) - E^n\left(V^n_{\mathrm{unrel}}(x)\right)\right\}. \quad (14)$$

Here, $V^n(x)$ denotes the volume of a tetrahedron of structure n, but equilibrated in a random alloy of volume $V_{\mathrm{rand}}(x)$. $V^n(x)$ is approximated by calculating diatomic lengths A-A, A-B, and B-B in the random medium (with bulk moduli instead of atomic force constants), and combining these to get the total volume of each tetrahedron type. $E^n\left(V^n_{\mathrm{rel}}(x)\right)$ is the value of the equation of the state of structure n at the *equilibra.46822 1 Tf 02.947(lf 0.4639 0 0 Tof)- 9.97 0 E*

E. Selection of input structures and interactions

Regarding point (v), the choice of pair figures is facilitated by the constrained fit Eq. (8) above. However, in earlier work[9,10,13,16,18] the choice of relevant many-body figures required tedious comparison of predicted and actual properties of an alloy to ensure that the optimum fit had been chosen. In this process, additional LDA input structures were introduced as needed, e.g., as ground-state structures of some previous prediction, but might also be excluded again if they were too high in energy and could not be fit accurately.[10]

IV. OPTIMIZED APPROACH TO THE SELECTION OF INPUT STRUCTURES AND FIGURES

A. Leave-many-out cross-validation

As mentioned above, the most promising technique to judge the predictive power of a CE from *within* a given set of input $\mathsf{D}H_{\mathrm{LDA}}\ \boldsymbol{\sigma}$ [problem (iv)] is *cross-validation*. However the two previously used approaches may either be prone to overoptimization (HOS-CV

V. DETERMINISTIC CLUSTER EXPANSION OF MO-TA

A. Constructing the MBCE input: LDA calculations

To obtain the MBCE parameters defined in Eq. (3) as described in the preceding section, we require two distinct types of input from total-energy calculation: The formation enthalpies $\Delta H_{\mathrm{LDA}}(\boldsymbol{\sigma})$ for a set of selected input configurations $\boldsymbol{\sigma}$ including full structural relaxation, and the corresponding constituent strain contribution $E_{\mathrm{ref}}(\boldsymbol{\sigma})$.

pounds were obtained in the LDA to density-functional theory, using the momentum-space total-energy method[48] as implemented in the VASP prog0 T6on4prog0 ,

Theory2obtai6(T)enl2obtaiillut ,A-

IV lists all LDA-calculated input structures for Mo-Ta, together with their formation enthalpies and the iteration in which they were first introduced. The input for iteration 1 consisted of a set of 24 structures, marked "1" in the last column of Table IV. In iterations 2–5, the input set was increased to 34, 43, 49, and 56 structures, respectively, with the additions in each iteration also marked in Table IV. In each iteration, the pool of many-body figures from which candidate CE's were selected comprised 47 candidate clusters: 13 inequivalent three-body terms up to fifth-nearest-neighbor maximum intersite separation, 27 inequivalent four-body figures up to fourth-nearest-neighbor maximum intersite separation, 4 inequivalent five-body figures up to third-nearest-neighbor intersite separation, and the smallest six-body figure, the octahedron (third-nearest-neighbor intersite separation). As examples, Fig. 6 shows the optimum many-body figures used for the final Mo-Ta MBCE: four three-body figures and one four-body figure, extending up to fifth-nearest-neighbor intersite separation at most. In a final step, the optimum CE of iteration 5 was refined once more using the same LDA data base, but by applying fit weights of 10 to the CE ground-state structures. This procedure improved the representation of this particularly interesting region of our without severe impact to other areas of the fit.

Figure 7 illustrates the LMO-CV score for the optimum MBCE of each iteration. LMO-CV scores for different iterations are not directly comparable numerically since the input structure set changes, and prediction sets are freshly chosen each time. Nevertheless, an interesting trend is apparent: the numerical values of s_{cv} do not fluctuate very much as the LDA structure base increases. Only the scatter of individual prediction set errors around their average is somewhat reduced.

It is interesting to compare the development of s_{cv} [Eq. (15)] to that of the least-squares fit error, s_{lsq} [Eq. (7)], tabulated in Table II for each successive iteration: s_{lsq} is always clearly smaller than s_{cv}, i.e., of little value to gauge a CE's predictive performance. To assess the latter, we can use our *a posteriori* knowledge of the complete LDA input set (Table IV in Appendix A). We may compare s_{cv} of each iteration to the averaged prediction errors for those structures not yet in the LDA data base. These values are termed s_{real} in Table II, and can be directly compared with s_{cv}. While of the same order of magnitude, s_{real}

A2 states is theoretically well understood as a model second-order transition. For this case, both the analytic (series-expansion) limit[58] and early Monte Carlo simulations[59] agree on a transition temperature $k_B T_c = 6.35 J_{nn}$. Since the nearest neighbor interaction J_{nn} is the clearly dominant term of our Mo-Ta MBCE [Fig. 8(a)], it would seem natural that a simple nearest-neighbor-only formula should give a good idea of the true A2-B2 T_c. In this approximation, $D_{nn} J_{nn} = 108$ meV of Mo-Ta corresponds to a T_c of almost 2000 K. This conflicts with experiment, since the published phase diagram reports only a continuous A2 solid solution, and early x-ray diffraction measurements[60] revealed no superstructure for samples sintered either at 1773 K 5 h or 673 K 100 h . Ordering might have been inhibited at 673 K since diffusion in Mo-Ta is slow,[61] but should have been sufficiently fast at 1773 K.

This failure can be related to the neglected high-order pair and many-body interactions of real Mo-Ta. To verify this, we performed canonical Monte Carlo simulations using our converged MBCE Hamiltonian. We used $Mo_{0.5}Ta_{0.5}$ supercells sized up to 32 3 32 3 32 unit cells, cooling down stepwise from the high-T solid solution into the B2-ordered regime, with 2000 or 4000 spin flips per site and step for proper equilibration. Figure 9 displays the resulting mixing enthalpy ΔH_{CE} and the configurational heat capacity C_v for 16 3 16 3 16 supercells. The Monte Carlo simulation agrees with Ref. 59 when restricted to the nearest-neighbor-only approximation [Fig. 9(a)]: As expected for a second-order transition, $\Delta H_{nn\text{-}only}$

$$\Delta H_{\mathrm{mix}}(x,\ldots) = J_0 + (2x-1)\,J_1 + \sum_{\mathrm{pairs}} (2x-1)^{2} D_{\mathrm{pair}} J_{\mathrm{pair}} + \sum_{\mathrm{MBs}} (2x-1)^{l} D_{\mathrm{MB}} J_{\mathrm{MB}} + \int_{V} \Delta E_{\mathrm{CS}}^{\mathrm{eq}}(\hat{k},x)\,d^{2}$$

metric B2 MoTa and a nearest-neighbor-only model in Fig. 9(a).

Experimentally, diffuse intensity measurements along the (000)-(400) line on Mo-Ta for $x = 21\%$, 37%, and 91% have been reported by Predmore and Arsenault.[24] These authors presented uncorrected diffraction data (i.e., a_{SRO} is overlaid by fundamental Bragg peaks, thermal scattering, lattice distortion, etc.)

cluster expansion of Mo-Ta. Both direct LDA calculations and the fitted cluster expansion formation enthalpies are listed. Structures are defined either by a common name, or in a superlattice notation. For the cases where neither nomenclature exists, the actual lattice occupation is described in Appendix B.

APPENDIX B: DEFINITION OF NONSUPERLATTICE LDA INPUT STRUCTURES IN TABLE IV

The present section defines those LDA input structures (Table IV) which have no common name, and cannot be described by a superlattice notation. To emphasize the connection between superstructure and underlying bcc lattice, atomic coordinates are given in Cartesian coordinates, in units of the (cubic) bcc lattice parameter, and without relaxation.

1. A_8B

Description: This structure is a body-centered tetragonal "3 3 3 3 1" defect cell of minority atoms embedded in the majority matrix.

Space group: $I4/mmm$ (No. 139 in the International Tables for Crystallography[66]).

Primitive cell (Cartesian coordinates):

$a_1 = 1.0, 0.0, 0.0$, $a_2 = 0.5, 1.5, 1.5$, $a_3 = 0.5, -1.5, 1.5$

Atomic coordinates (Cartesian coordinates):

A_1: 1.0, −1.0, 1.0 , A_2: 0.5, −0.5, 0.5 , A_3: 0.5, 0.5, 0.5 , A_4: 0.5, −0.5, 1.5 , A_5: 1.0, 0.0, 1.0 , A_6: 1.0, 1.0, 1.0 , A_7: 1.0, 0.0, 2.0 , A_8: 0.5, 0.5, 1.5 , B_1: 0.0, 0.0, 0.0 .

2. A_7B

Description: This structure is a primitive tetragonal defect cell of minority atoms embedded in the majority matrix, in a sequence of one c 2 3 2 (100) AB plane followed by three pure A planes.

Space group: $P4/mmm$ (No. 123 in the International Tables for Crystallography[66]).

Primitive cell (Cartesian coordinates):

$a_1 = 1.0, -1.0, 1.0$, $a_2 = 1.0, 1.0, 0.0$, $a_3 = 0.0, 0.0, 2.0$

Atomic coordinates (Cartesian coordinates):

A_1: 1.0, 0.0, 0.0 , A_2: 0.5, −0.5, 0.5 , A_3: 0.5, 0.5, 0.5 , A_4: 0.0, 0.0, 1.0 , A_5: 1.0, 0.0, 1.0 , A_6: 0.5, −0.5, 1.5 , A_7: 0.5, 0.5, 1.5 , B_1: 0.0, 0.0, 0.0 .

3. $A_{12}B_4$-I

Description: This is a body-centered tetragonal structure of (100)-oriented, pure B, and alternating AB columns embedded into an A matrix.

Space group: $I4_1/amd$ (No. 141 in the International Tables for Crystallography[66]).

Primitive cell (Cartesian coordinates):

$a_1 = 2.0, 0.0, 0.0$, $a_2 = 0.0, 2.0, 0.0$, $a_3 = 1.0, 1.0, 2.0$

Atomic coordinates (Cartesian coordinates):

A_1: 0.0, 1.0, 0.0 , A_2: 1.0, 1.0, 0.0 , A_3: 0.5, 0.5, 0.5 , A_4: 0.5, 1.5, 0.5 , A_5: 1.5, 0.5, 0.5 , A_6: 1.5, 1.5, 0.5 , A_7: 2.0, 1.0, 1.0 , A_8: 2.0, 2.0, 1.0 , A_9: 1.5, 1.5, 1.5 , A_{10}: 2.5, 2.5, 1.5 , A_{11}: 2.5, 1.5, 1.5 , A_{12}: 1.5, 2.5, 1.5 , B_1: 0.0, 0.0, 0.0 , B_2: 1.0, 0.0, 0.0 , B_3: 1.0, 1.0, 1.0 , B_4: 1.0, 2.0, 1.0 .

4. $A_{12}B_4$-II

Description: This is a cubic structure with 2 3 2 3 2 unit cell.

Space group: $Pm\bar{3}m$ (No. 221 in the International Tables for Crystallography[66]).

Primitive cell (Cartesian coordinates):

$a_1 = 2.0, 0.0, 0.0$, $a_2 = 1.0, 2.0, 0.0$, $a_3 = 1.0, 1.0, 2.0$

Atomic coordinates (Cartesian coordinates):

A_1: 0.0, 1.0, 0.0 , A_2: 1.0, 1.0, 0.0 , A_3: 0.5, 0.5, 0.5 , A_4: 0.5, 1.5, 0.5 , A_5: 1.5, 0.5, 0.5 , A_6: 1.5, 1.5, 0.5 , A_7: 2.0, 1.0, 1.0 , A_8: 2.0, 2.0, 1.0 , A_9: 1.5, 1.5, 1.5 , A_{10}: 2.5, 2.5, 1.5 , A_{11}: 2.5, 1.5, 1.5 , A_{12}: 1.5, 2.5, 1.5 , B_1: 0.0, 0.0, 0.0 , B_2: 1.0, 0.0, 0.0 , B_3: 1.0, 1.0, 1.0 , B_4: 1.0, 2.0, 1.0 .

40756.985 40756.9897664)

Space group: $R\bar{3}m$ (No. 166 in the International Tables for Crystallography[66]).

Primitive cell (Cartesian coordinates):

$a_1 =$

7. Mo_4Ta_{12}

Description: This structure can not be described by a superlattice notation. It has a simple tetragonal cell.

Space group: $P4_2/mnm$ (No. 136 in the International Tables for Crystallography[66]).

Pearson symbol: $tP24$

Unit-cell parameters (primitive cell):

$a=3.178$ Å, $b=9.152$ Å, $c=9.152$ Å

$\alpha=90.00°$, $\beta=90.00°$, $\gamma=90.00°$

Fractional atomic coordinates:

Mo_1: 0.000,0.001,0.001 , Mo_2: 0.000,0.749,0.749 , Mo_3: 0.500,0.249,0.501 , Mo_4: 0.500,0.501,0.249 , Ta_1: 0.000,0.008,0.497 , Ta_2: 0.000,0.253,0.742 , Ta_3: 0.000,0.255,0.255 , Ta_4: 0.000,0.495,0.495 , Ta_5: 0.000,0.497,0.008 , Ta_6: 0.000,0.742,0.253 , Ta_7: 0.500,0.242,0.997 , Ta_8: 0.500,0.508,0.753 , Ta_9: 0.500,0.753,0.508 , Ta_{10}: 0.500,0.755,0.995 , Ta_{11}: 0.500,0.995,0.755 , Ta_{12}: 0.500,0.997,0.242 .

APPENDIX D: DEFINITION OF BCC SPECIAL QUASIRANDOM STRUCTURES

The present section defines the body-centered cubic (special) quasirandom structures used to verify the MBCE-predicted random alloy enthalpy of mixing in Sec. VI C (Fig. 10). To emphasize the connection between superstructure and underlying bcc lattice, atomic coordinates are given in Cartesian coordinates, in units of the (cubic) bcc lattice parameter, and without relaxation.

1. SQS-16 $A_{0.75}B_{0.25}$

Description: This is the only bcc-based structure with 16 atoms per unit cell and $x=25$ which satisfies $\Pi_p \sigma = 0.25$ for the first four pair correlation functions. It has a base-centered monoclinic unit cell.

Space group: Cm (No. 8 in the International Tables for Crystallography[66]).

Primitive cell (Cartesian coordinates):

$a_1=$ 2.1,−2.0,0.0 , $a_2=$ 1.0,1.0,0.0 , $a_3=$ 1.0,0.0,2.0

Atomic coordinates (Cartesian coordinates):

A_1: 1.0,0.0,0.0 , A_2: 1.0,−1.0,0.0 , A_3: 2.0,−1.0,0.0 , A_4: 2.5,−1.5,0.5 , A_5: 2.5,−0.5,0.5 , A_6: 2.0,−1.0,1.0 , A_7: 2.0,0.0,1.0 , A_8: 3.0,−1.0,1.0 , A_9: 1.5,−0.5,1.5 , A_{10}: 1.5,0.5,1.5 , A_{11}: 2.5,−1.5,1.5 , A_{12}: 2.5,−0.5,1.5 , B_1: 0.0,0.0,0.0 , B_2: 1.5,−0.5,0.5 , B_3: 1.5,0.5,0.5 , B_4: 1.0,0.0,1.0 .

2. SQS-16 $A_{0.50}B_{0.50}$

Description: There are no structures with less than 16 atoms per unit cell and $x=0.5$ which satisfy $\Pi_p \sigma = 0.0$ for the first five pair correlation functions, but twelve different 16-atom structures satisfy this criterion. The SQS selected here is subject to the additional criterion that the least-squares sum over some of the remaining, nonzero short-range correlation functions (

Holland, Amsterdam, 1991).
[7] J. Sanchez and D. de Fontaine, in *Structure and Bonding in Crystals*, edited by M. O'Keefe and A. Navrotsky (Academic, New York, 1981), Vol. 2, p. 117.
[8] J. Sanchez, F. Ducastelle, and D. Gratias, Physica A **128**, 334 (1984).
[9] A. Zunger, in *Statics and Dynamics of Alloy Phase Transformations*, edited by P. Turchi and A. Gonis (Plenum, New York, 1994), pp. 361–419.
[10] A. Zunger, L. Wang, G. Hart, and M. Sanati, Modell. Simul. Mater. Sci. Eng. **10**, 1 (2002).
[11] L. Ferreira, S.-H. Wei, and A. Zunger, Phys. Rev. B **40**, 3197 (1989).
[12] J. Connolly and A. Williams, Phys. Rev. B **27**, 5169 (1983).
[13] L. Ferreira, S.-H. Wei, and A. Zunger, Int. J. Supercomput. Appl. **5**, 34 (1991).
[14] Z. Lu, S.-H. Wei, A. Zunger, S. Frota-Pessoa, and L. Ferreira, Phys. Rev. B **44**, 512 (1991).
[15] Z. Lu, D. Laks, S.-H. Wei, and A. Zunger, Phys. Rev. B **50**, 6642 (1994).
[16] V. Ozoliņš, C. Wolverton, and A. Zunger, Phys. Rev. B **57**, 6427 (1998).
[17] C. Wolverton, V. Ozoliņš, and A. Zunger, Phys. Rev. B **57**, 4332 (1998).
[18] S. Müller, L.-W. Wang, A. Zunger, and C. Wolverton, Phys. Rev. B **60**, 16 448 (1999).
[19] M. Sanati, L. Wang, and A. Zunger, Phys. Rev. Lett. **90**, 045502 (2003).
[20] D. Laks, L. Ferreira, S. Froyen, and A. Zunger, Phys. Rev. B **46**, 12 587 (1992).
[21] M. Plutowski, *Survey: Cross-validation in Theory and Practice*, http://www.emotivate.com/CvSurvey.doc (1996).
[22] A. van de Walle and G. Ceder, J. Phase Equilib. **23**, 348 (2002).
[23] V. Blum and A. Zunger, Phys. Rev. B **69**, 020103 (2004).
[24] B. Predmore and R. Arsenault, Scr. Metall. **4**, 213 (1970).
[25] S. Singhal and W. Worrell, in *Proceedings of the International Symposium on Metallurgical Chemistry, Brunel University and National Physical Laboratory, UK, 1971*, edited by O. Kubaschewski (Her Majesty's Stationary Office, London, 1974), pp. 65–72.
[26] S. Singhal and W. Worrell, Metall. Trans. **4**, 1125 (1973).
[27] S. Singhal and W. Worrell, Metall. Trans. **4**, 895 (1973).
[28] C. Colinet, A. Bessoud, and A. Pasturel, J. Phys. F: Met. Phys. **18**, 903 (1988).
[29] C. Colinet and A. Pasturel, Physica B **159**, 275 (1989).
[30] C. Sigli and J. Sanchez, Acta Metall. **36**, 367 (1988).
[31] *Phase Equilibria, Crystallographic and Thermodynamic Data of Binary Alloys*, Vol. 5H of *Landolt-Börnstein, New Series, Group IV*, edited by B. Predel (Springer, Berlin, 1997).
[32] P. Turchi, A. Gonis, V. Drchal, and J. Kurdnovsky, Phys. Rev. B **64**, 085112 (2001).
[33] A. Carlsson, Phys. Rev. B **35**, 4858 (1987).
[34] A. Carlsson and J. Sanchez, Solid State Commun. **65**, 527 (1988).
[35] A. Carlsson, Phys. Rev. B **40**, 912 (1989).
[36] T. Mohri, K. Terakura, S. Tazikawa, and J. Sanchez, Acta Metall. Mater. **39**, 493 (1991).
[37] A. Pasturel, C. Colinet, A. Paxton, and M. van Schilfgaarde, J. Phys.: Condens. Matter **4**, 945 (1992).
[38] G. Rubin and A. Finel, J. Phys.: Condens. Matter **7**, 3139 (1995).
[39] G. Das, A. Arya, and S. Banerjee, Intermetallics **4**, 625 (1996).
[40] Y. Chen, T. Atago, and T. Mohri, J. Phys.: Condens. Matter **14**, 1903 (2002).
[41] C. Wolverton, V. Ozoliņš, and A. Zunger, J. Phys.: Condens. Matter **12**, 2749 (2000).
[42] J. E. Bernard, L. G. Ferreira, S.-H. Wei, and A. Zunger, Phys. Rev. B **38**, 6338 (1988).
[43] G. P. Srivastava, J. L. Martins, and A. Zunger, Phys. Rev. B **31**, 2561 (1985).
[44] A. Ruban, S. Simak, S. Shallcross, and H. Skriver, Phys. Rev. B **67**, 214302 (2003).
[45] Z. Lu, S.-H. Wei, and A. Zunger, Phys. Rev. B **45**, 10 314 (1992).
[46] S.-H. Wei, A. Mbaye, L. Ferreira, and A. Zunger, Phys. Rev. B **36**, 4163 (1987).
[47] J. Shao, J. Am. Stat. Assoc. **88**, 486 (1993).
[48] J. Ihm, A. Zunger, and M. Cohen, J. Phys. C **12**, 4409 (1979).
[49] G. Kresse and J. Furthmüller, Phys. Rev. B **54**, 11 169 (1996).
[50] G. Kresse and J. Furthmüller, Comput. Mater. Sci. **6**, 15 (1996).
[51] P. Blöchl, Phys. Rev. B **50**, 17 953 (1994).
[52] G. Kresse and A. Joubert, Phys. Rev. B **59**, 1758 (1999).
[53] J. Perdew and A. Zunger, Phys. Rev. B **23**, 5084 (1981).
[54] H. Monkhorst and J. Pack, Phys. Rev. B **13**, 5188 (1976).
[55] S. Froyen, Phys. Rev. B **39**, 3168 (1999).
[56] P. Blöchl, O. Jepsen, and O. Andersen, Phys. Rev. B **49**, 16 223 (1994).
[57] P. Blaha, K. Schwarz, and J. Luitz, WIEN97 (TU Wien, Vienna, 1999).
[58] D. Gaunt, Proc. Phys. Soc. London **92**, 150 (1967).
[59] D. Landau, Phys. Rev. B **16**, 4164 (1977).
[60] G. Geach and D. Summers-Smith, J. Inst. Met. **80**, 143 (1952).
[61] F. Guillemot, M. Boliveau, M. Bohn, J. Debuigne, and D. Ansel, Int. J. Refract. Met. Hard Mater. **19**, 183 (2001).
[62] A. Zunger, S.-H. Wei, L. Ferreira, and J. Bernhard, Phys. Rev. B **65**, 353 (1990).
[63] C. Sigli, M. Kosugi, and J. Sanchez, Phys. Rev. Lett. **57**, 253 (1986).
[64] Z. Bangwei and O. Yifang, Phys. Rev. B **48**, 3022 (1993).
[65] J. Perdew and Y. Wang, Phys. Rev. B **45**, 13 244 (1992).
[66] *International Tables for Crystallography*, Vol. A, edited by T. Hahn (D. Reidel, Dordrecht, 1983).
[67] *Pearson's Handbook of Crystallographic Data for Intermetallic Phases, 2nd ed.*, edited by P. Villars and L. Calvert (ASM International, Materials Park, OH, 1991).